Tikrit Journal of Engineering Sciences (2025); 32(3): 1870
DOI: http://doi.org/10.25130/tjes.32.3.2

IRAQI Academic Scientific Journals

ISSN: 1813-162X (Print); 2312-7589 (Online)
Tikrit Journal of Engineering Sciences
available online at: http://www.tj-es.com

TJES Tikrit Journal of Engineering Sciences

Removal of Phosphate Ions from Aqueous Solution by Al2O3 Nanoparticles Loaded on Activated Carbon Synthesized from Aloe Vera Gum

Ghalib J. K. Al-Sumaidaie *[a], **Muzher M. I. AL-Doury** [b]

[a] Department of Chemical Engineering, College of Engineering, Tikrit University, Tikrit, Iraq.
[b] Petroleum and Gas Refining Engineering Department, Petroleum Processes Engineering College, Tikrit University, Tikrit, Iraq.

Keywords:
Phosphate; AL_2O_3/ABGAC; Al_2O_3 NPs; Fly ash; Magnetic field Strength; Wavelength.

Highlights:

- Preparation of Al_2O_3/Aloe vera Barbadensis Gum Activated Carbon (ABGAC).
- Test the performance of this adsorbent under various operating parameters.

ARTICLE INFO

Article history:

Received	12 Nov. 2023
Received in revised form	19 Jan. 2024
Accepted	18 July 2024
Final Proofreading	05 Apr. 2025
Available online	17 June 2025

Citation: Al-Sumaidaie GJK, AL-Doury MMI. **Removal of Phosphate Ions from Aqueous Solution by Al2O3 Nanoparticles Loaded on Activated Carbon Synthesized from Aloe Vera Gum**. *Tikrit Journal of Engineering Sciences* 2025; **32**(3): 1870.
http://doi.org/10.25130/tjes.32.3.2

*Corresponding author:
Ghalib J. K. Al-Sumaidaie
Department of Chemical Engineering, College of Engineering, Tikrit University, Tikrit, Iraq.

Abstract: A prepared Aluminum Oxide AL_2O_3 nanoparticle loaded on Aloe vera Barbadensis Gum Activated Carbon (ABGAC) using the sol-gel method to increase the surface area is employed for phosphate removal from synthetic aqueous solutions. The operating parameters in this study are pH 3-9, adsorbent dose of AL_2O_3/ABGAC 20-100 mg per 1-liter solution, contact time (CT) 5-105 minutes, magnetic field strength (MFS) 300-600 mTesla, wavelength of light is halogen lamp (white, green, red, yellow, blue, and sunlight), and initial phosphate concentration (C_i) 3.7-10.7 mg/L. The results indicated that phosphate can be removed efficiently with the highest removal efficiency of 85.52% under the following operating conditions: pH= 5, CT= 105 min, Dose= 60 mg, MFS= 600 mTesla, red light, and C_i = 7.6 mg/L. It has been proved that the Langmuir model significantly fits the experimental data. The obtained adsorption capacity range was 63.24 - 969.38 mg/g.

إزالة ايونات الفوسفات من محلول مائي باستخدام الجسيمات النانوية Al2O3المحملة على الكاربون المنشط المحضر من جل الصبار

غالب جاسم كاظم الصميدعي[1]، مزهر مهدي إبراهيم الدوري[2]

[1] قسم الهندسة الكيمياوية/ كلية هندسة / جامعة تكريت/ تكريت – العراق.

[2] قسم هندسة تكرير النفط والغاز/ كلية هندسة العمليات النفطية / جامعة تكريت/ تكريت – العراق.

الخلاصة

تم استخدام مادة اوكسيد الألومنيوم Al_2O_3 النانوية المحملة على الكاربون المنشط المحضر من صمغ نبات الصبار (ABGAC)، وهو مادة طبيعية تفرز من أساسها صبار باربادنسيس لتكوين مركبات نانوية باستخدام طريقة سول – جل لغرض زيادة المساحة السطحية لإزالة الفوسفات من محلول مائي مصنع. تم استخدام الظروف التشغيلية التالية: الرقم الهيدروجيني ٣-٩، الجرعة المادة المازة (Al2O3/ABGAC) ١٠٠-٢٠ ملغم)، وقت التلام 5-105 دقيقة، قوة المجال المغناطيسي 300-600 ملي تسلا، الطول الموجي للضوء باستخدام مصباح الهالوجين (الأبيض والأخضر والأحمر والأصفر والأزرق وضوء الشمس) وتركيز الفوسفات 3.7-10.7 ملغم / لتر. تم إجراء تجارب الدفعة الواحدة باستخدام جهاز Hanna Phosphate High-Range Checker وجهاز اختبار الجرة. أشارت النتائج إلى أن أعلى كفاءة إزالة للفوسفات هي ٨٥,٥٢٪ تحت ظروف التشغيل التالية: الرقم الهيدروجيني ٥، وقت التلامس ١٠٥ دقيقة، الجرعة ٦٠ ملغ، شدة المجال المغناطيسي ٦٠٠ ملي تسلا، الضوء الأحمر، ولتركيز فوسفات 7.6 ملغم / لتر. لقد وجد أن نموذج الامتزاز لانجمير يتناسب تماما مع البيانات التجريبية، وقد بلغت سعة الامتزاز ٦٣,٢٤ - ٩٦٩,٣٨ ملجم/جم.

الكلمات الدالة: الفوسفات؛ AL2O3/ABGAC؛ جسيمات نانوية من Al2O3؛ الرماد المتطاير؛ قوة المجال المغناطيسي؛ الطول الموجي.

1.INTRODUCTION

Phosphate plays an important role in the eutrophication process since it leads to excessive generation of organic matter due to the over-enrichment of nutrients in water bodies, resulting in a decline in water quality [1], elucidating the aspiration to eliminate phosphate from aqueous solutions [2]. Significant quantities of phosphates are lost to aquatic environments, land disposal sites, and facilities for treating aqueous solutions [3]. Several technologies are used for phosphate removal from aqueous solutions, including chemical technologies, such as coagulation and flocculation, mineral precipitation, and crystallization [4]; biological treatment using activated sludge or algae-based treatment [5]; and Physical processes, such as Reverse Osmosis (RO), membrane purification, ion exchange and adsorption [6]. The most well-known process is thought to be adsorption. There is an urgent need for cost-effective and ecologically sustainable methods; therefore, developing novel adsorbents is imperative. Several adsorbents have been used for this purpose, including zirconium oxide, nanostructured binary oxides, and metal-organic structures (MOFs), i.e., metal-organic frameworks [7]. Lin et al. [8] were the first to investigate the efficacy of a functionalized MOF in phosphate adsorption. They examined the impact of an amino group on phosphate removal from water using a zirconium-based MOF. The removal efficiency of UiO-66-NH2 was higher than that of UiO-66 due to the presence of the amine functional group, the highest removal efficiency (94%) at 25 °C and pH = 4, while UiO-66, UiO-66-NO_2 and UiO-66-Br exhibited a maximum removal efficiency of (74.5%, pH=4), (89%, pH=4), and (91 %, pH=5), respectively. Since that date, much work has been done to remove phosphates from aqueous solutions using different MOFs. Wang et al. [9] removed phosphate using prepared nanoparticles by loading Fe_3O_4 onto the zirconia envelope prepared by a one-step co-precipitation method with an applicating magnetic field. They found that the Langmuir model and the pseudo-second-order fitted the experimental data. The removal efficiency decreased with the increase of the pH above 5.5 due to replacing hydroxyl groups. The adsorption capacity increased with the dose of the adsorbent. The highest removal efficiency was 85% at a contact time of 20 minutes. Zhang et al. [10] showed that the Langmuir model fitted the experimental data. The highest removal (89%) was under acidic conditions (pH 4.0). The results of Itrogiannis et al. [11] indicated that the process was chemisorption and the pseudo-second-order kinetic model fitted experimental data of phosphate adsorption onto Zr (IV)-AS, meaning that the adsorption process was of chemisorption. Batch and column experiments were conducted by Xiong et al. [12] using zirconium-modified activated sludge (Zr (IV)-AS) to assess the adsorbent composites' structural and physiochemical properties. To test the effect of LED radiation on phosphate removal, Manikandan et al. [13] synthesized the adsorbent by loading titanium dioxide molecules on activated carbon. It was found that red light was more effective than other colors in removing phosphates, causing a removal efficiency of 96% at a contact time of 75 minutes. Al_2O_3 nanoparticles possess distinctive characteristics that render them suitable for diverse applications, such as water remediation, biomedical applications, and catalysts [14]. Natural gums, such as peach gum and seed gum, have been used to remove pollutants, including hydrocarbon fraction and synthetic dyes. Mukherjee et al. [15] used guar gum to treat lead from aqueous solutions. Sahraei et al. [16] used a modified biopolymer gum to remove dyes and heavy metals from

aqueous solution. Aloe vera gum is a naturally occurring polysaccharide secreted from the "drumstick tree" (Aloe vera Barbadensis), a prevalent tree species distributed throughout tropical and subtropical regions worldwide**.** The main goal of this work is to remove phosphates from an aqueous solution with a promising and environmentally friendly adsorbent, i.e., Al_2O_3/ABGAC nanocomposites (Alumina Nanoparticles on Aloe vera Barbadensis Gum Activated Carbon (ABGAC)). The operating parameters studied in this study were pH 3-9, adsorbent dose (Al_2O_3/ABGAC) nanoparticles (20-100 mg), contact time (CT) (5-105 minutes), magnetic field strength (MFS) (300-600 mTesla), wavelength of light using halogen lamp (white, green, red, yellow, blue, and sunlight), and initial ion concentration (Ci) (3.7-10.7 mg/L).

2.APPARATUS, MATERIALS, AND PROCEDURES

2.1.Apparatus

A programmable jar tester supplied by Phipps & Bird PB-900, made in the USA, was employed to conduct the present work. Hanna Phosphate High Range Checker® was used to measure phosphate concentration. It utilized a fixed-wavelength LED and a silicon photodetector to achieve precision comparable to professional-grade instruments while remaining cost-effective compared to traditional chemical test kits.

2.2.Materials

2.2.1.Preparation of Aloe Vera Barbadensis Gum Activated Carbon (ABGAC)

The Aloe vera Barbadensis Gum was collected and subjected to desiccation through exposure to sunlight, after which it was pulverized into a fine powder. The ABGAC powder was incorporated into a concentrated solution of H_2SO_4 (50%) in a ratio of 2:1 (v/w). The resulting mixture was continuously stirred until a uniform consistency was achieved. Subsequently, the material underwent a drying process followed by thermal activation through heating at 600 °C for 2 hours, isolated from air and without nitrogen using the muffle furnace from SNOL. The product was placed in a heat-resistant metal crucible and tightly closed, as shown in Fig. 1. Then, successive washing with deionized water was performed until the attainment of the supernatant to eliminate surplus acidity. The sample was subjected to a 2% $NaHCO_3$ (w/v) solution to eliminate residual acid, followed by a thorough rinsing with deionized water. The specimen was desiccated via a hot air oven set at 105 °C for 8 hours. The bio-sorbent was subjected to a sieving process to achieve a uniform particle size internal structure of 39-47 nm, after which it was carefully stored in an airtight container for subsequent utilization [17].

Fig. 1 Muffle Furnace from SNOL.

2.2.2.Preparation of Al_2O_3/ABGAC Nanocomposites

Sol-gel synthesis was used to prepare the Al_2O_3/ABGAC nanocomposites. Continuous stirring was used to combine 2.5 grams of $Al_2(SO_4)_3$ with 3 grams of ABGAC at room temperature for 30 minutes. About 10 mL of NaOH (0.1 M) solution was added drop by drop, and the mixture was stirred constantly for 1 hour to achieve a highly homogeneous solution. After the solution was homogenized, it was filtered and rinsed multiple times with ethanol and deionized water. Water and organic residues were removed from the obtained gel by drying at 110 °C for 5 hours. The sample was milled into a powder to eliminate lumps. Al_2O_3/ABGAC nanocomposites were produced by calcining the obtained powder in a muffle furnace at 800 °C for 2 hours, done in isolation from air [18]. The surface area and pore volume distribution of the produced catalyst were measured using multi-point Brunauer, Emmett, and Teller (BET) techniques. Moreover, XRD and SEM were done in the Oil Research and Development Center, Ministry of Oil, and Alkhora company nano research laboratories. Careful inspection of Figs. 2, 3, and 4 indicated that ABGAC had a flakes internal structure of 39-47 nm size, Al_2O_3/ABGAC had a nearly spherical internal structure of 43-97 nm size, while Al_2O_3 NPs had a homogeneous spherical structure of 50 nm size. Although Al_2O_3/ABGAC did not have a smaller particle size, it had a higher surface area according to BET analysis (Table 1), and it acquired the highest removal due to its composition being most attractive to phosphate and its higher surface area, providing more adsorption sites. Bun-ichi [19] stated that the

adsorption process depends on the nature and properties of adsorbent and adsorbate. Adsorbent properties include surface area, which increased with the decrease in particle size. Figure 5 shows that the peaks were sharp and high, typical of Al_2O_3/ABGAC indexed to the face of carbon comparison with shape in Figs. 6 and 7. The appearance of a broad, strong diffraction peak at 2θ values in the XRD spectrum showed that ABGAC had an amorphous and crystalline structure of 19.11°, 25.75°, 28.06°, 29.02°, 31.91°,38.12°, 32.7°, 41.13°, 48.48°, and 67.26°.

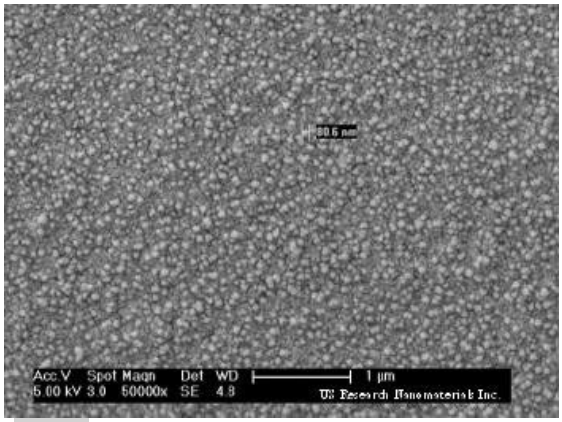

Fig. 2 SEM Image for α-Al_2O_3 Nanoparticles: the Sample Exhibits a Very Narrow Particle Size Range of 50 nm.

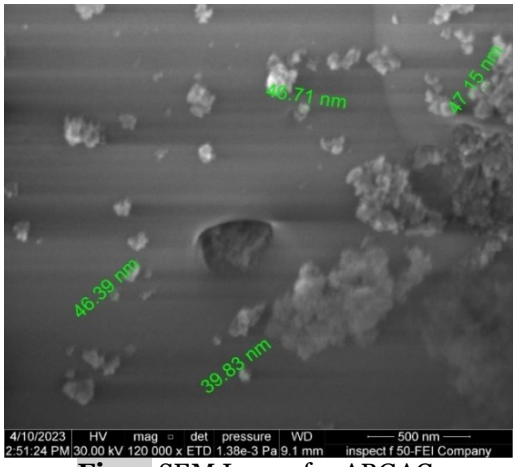

Fig. 3 SEM Image for ABGAC.

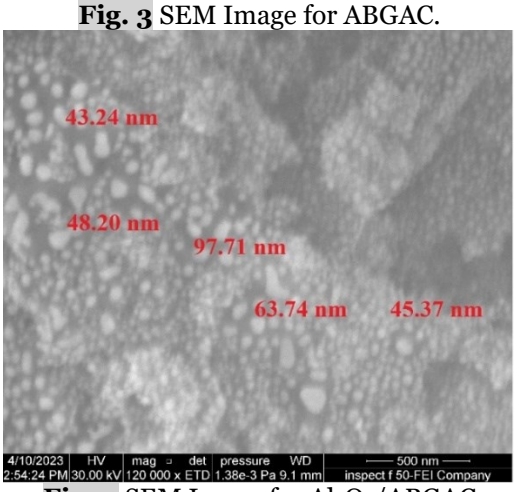

Fig. 4 SEM Image for Al_2O_3/ABGAC Nanocomposites.

Table 1 BET Analyses.

Sample name	Surface area, m^2/g	Method	Detection limit	Uncertainty value	Calibration (Internal or External)
Al_2O_3/ABGAC	124.255				
Al_2O_3 NPs	51.235	ISO 9277/2010	(0.1-2000)	0.182 %	Auto
ABGAC	56.438				

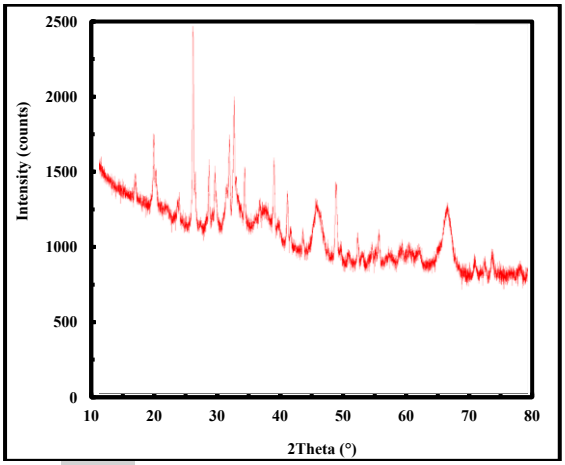

Fig. 5 XRD Pattern of Al_2O_3/ABGAC.

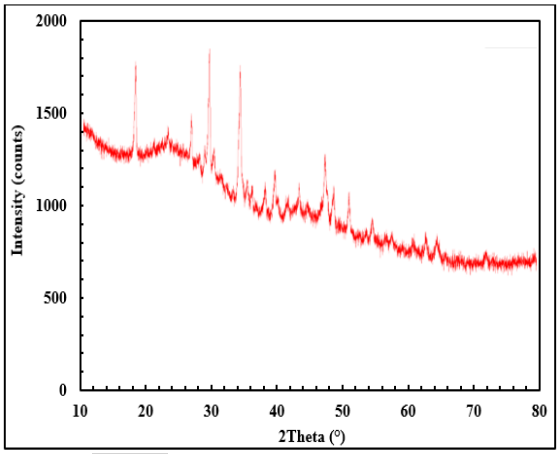

Fig. 6 XRD Pattern of ABGAC.

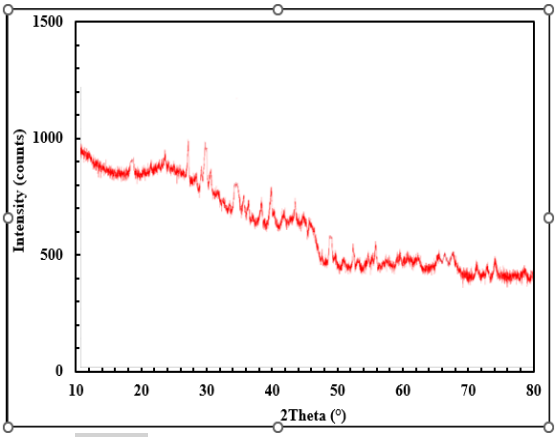

Fig. 7 XRD Pattern of Al2O3 NPs.

2.3.Experimental Procedure

One litter of synthetic PO_4^{-3} solution (3, 5, 7, and 10) mg was prepared using trisodium phosphate Na3PO4 . It is put into the cylinder and mixed for 10 minutes at 30 rpm. The pH was brought to the desired value with 0.1 M HCl or 0.1 M NaOH. The required dose of Al_2O_3/ABGAC nanocomposites was added, mixed quickly for 5 minutes at 250 rpm, then slowly mixed for 5 minutes at 30 rpm. Then, the study factors (concentration, dose, and pH) were changed. Then, the magnetic layers changed, i.e., to the bottom of the beaker from the outside. Also, the wavelength of light (white, green, red, yellow, blue, and sunlight) was changed using a halogen lamp. When the different light sources were illuminated with an electric current of 220 volts and a power of 20 watts, the experiments for sunlight were conducted during consecutive sunny days in March 2023 from 9.00 AM to 05.00 PM. The distance of the light source from the solution surface in the test was 3.00 cm. Take samples at different periods to measure the residual PO_4^{-3}. When the amount of phosphate was measured, it was found that there was an increase of 0.7 mg, which may be due to a simple factory defect in the device or a need for calibration, so the considered concentrations were (3.7, 5.7, 7.7, and 10.7) mg/L, i.e., the actual measured concentrations.

2.4.Experimental Sets

Adsorption is the process of moving a substance from the liquid or gaseous phase to the solid phase. There is physical, chemical, and mixed adsorption. When drawing the focus with time, an adsorption isotherm was produced. Several models represent it, such as Freundlich and Langmuir, BET, and others, which are the most famous models used. This process has applications in the fields of chemical and environmental engineering. The efficiency of the removal is calculated by Eq. (1).

$$\text{Removal Efficiency}(\%) = C_i\text{-}C_o/C_i \times 100 \quad (1)$$

As for the adsorption capacity, it is calculated in two ways: The first method according to Eq. (2)

$$\text{Adsorption Capacity} = (C_n\text{-}C_o)\,V/M \quad (2)$$

According to the model used, the Langmuir model was used for the second method, where C/(x/m) was drawn against (C_e). The resulting straight line is the intersection with the X axis representing 1/ ab, and the slope represents 1/a, i.e., a and b are the constants of Langmuir. To find the adsorption capacity, the incoming focus is projected on the X axis, goes up with a vertical line until the oblique line is cut, and then heads to the Y axis to click C/(x/m). Then, (x/m) is extracted, representing the adsorption capacity. The most important parameters influencing the processes are the initial concentration, dose of adsorbent Al_2O_3/ABGAC, contact time, pH, magnetic field intensity, and light wavelength. To cover the tested parameters, according to a full factorial set, 19200 experiments were required. Therefore, a semi-full Factorial set was followed. In the present work, seven experimental sets were followed. The purpose and range of the operating parameters are given in Table 2.

Table 2 Operating Parameters Range for the Studied Sets.

Set number	Purpose		Operating parameters						
			CT, minute	pH	Dose, mg	C_i, mg/l	MFS, mTesla	Wavelength	Adsorbent type
1	Test the effect of contact time (CT)		5-150	9	20-100	3.7-10.7	----	----	AL_2O_3/ABGAC
2	Test the effect of (pH)		105	3-9	20-100	3.7-10.7	-----	----	AL_2O_3/ABGAC
3	Test the effect of the initial Concentration (C_i)		105	5 and 9	20-100	3.7-10.7	----	----	AL_2O_3/ABGAC
4	Test the effect of the Dose		105	5	20-100	3.7-10.7	----	-----	AL_2O_3/ABGAC
5	Test the effect of MFS		105	5	60-100	3.7-10.7	300-600	-----	AL_2O_3/ABGAC
6	Test the effect of wavelength	First part	0-25hr	5	80,100	5.7, 10.7	600	red, blue	AL_2O_3/ABGAC
		Second part	8hr	5	60-100	3.7-10.7	600	White, green, red, yellow, sunlight, blue	AL_2O_3/ABGAC

3.RESULTS AND DISCUSSION

3.1.Effect of Contact Time

Figure 8 indicates that after only 30 minutes, approximately 33.36 % of the phosphate ions were adsorbed. The removal efficiency increased quickly with contact time up to about 100 minutes under most operating conditions. Then, it tended to level out. Therefore, 105 minutes of contact time was fixed for other experiments. At the beginning of the process, all adsorption sites were empty, and the driving force, i.e., the difference between the pollutant concentration at any time and the equilibrium concentration, was maximum, so the adsorption process was fast. As time proceeded, the pollutant concentration and the available empty adsorption sites were reduced, and the driving force was reduced, reducing the adsorption rate. Once the equilibrium was reached, no further adsorption occurred [20]. Khader et al. [21] stated that the adsorption was characterized by a fast stage at the beginning. Then, it was followed by a slow stage. At the start of adsorption, there were a lot of free available adsorption sites. However, as time proceeded, these sites were reduced gradually. Also, there was a repulsion between the pollutant and adsorbent. This result agrees well with [20-24]. The results showed that the maximum removal efficiency was 42.85% at 3.7 mg/L under initial PO_4^{-3} concentration, 80 mg Al_2O_3/ABGAC dose, and pH =9.

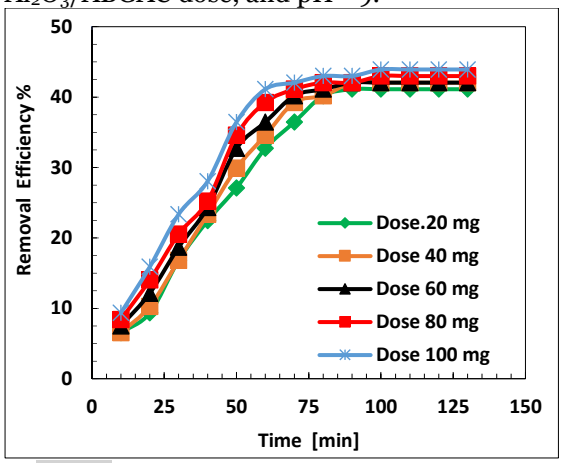

Fig. 8 Effect of Contact Time on Removal Efficiency, C_i 10.7 mg/L, and pH= 9.

3.2.Effect of pH

Figure 9 shows that the removal efficiency began with a gradual rise up to pH 5, after which it began to descend quickly to the lowest level at pH 9 due to the increasing competition between (OH^-) Phosphate groups and the adsorption sites. This trend is similar to that of [25]. Elkhaleefa et al. [26] and Ibrahim et al. [27] stated that pH is one of the most important parameters that can directly affect the adsorption process because it can affect the extent of ionization and the surface characteristics of an adsorbent. Abubakr et al. [26] also found that the adsorption increased till pH =5. Moreover, the adsorption rate decreased sharply for further increase of pH. The adsorption rate below pH 5 was reduced due to the high concentration of hydrogen ions. Moreover, the adsorption sites gained a positive charge, increasing the repulsive effects on the cations. For pH lower than 5, hydrogen ions (H^+) would stick on the adsorption sites, giving it a positive charge that reduced removal. For pH higher than 5, phosphate hydroxyl started to form, which is hardly adsorbed [12, 22, 28]. Alasadi et al. [29] mentioned that the attraction between the adsorbent and pollutant would affect the adsorption process. Cundari [14] stated that when the pH exceeded 5, phosphate (OH^-) started to form, which was badly absorbed. Also, when PO_4^{-3} was stuck to the surface of Al_2O_3, the acidity function difference was minor. A similar trend was found by [25, 20, 22]. Figure 9 indicates that the highest removal occurred under pH 5. The maximum removal efficiency was (68.42%) at 7.6 mg/L, initial concentration, dose of 60mg, and pH 5.

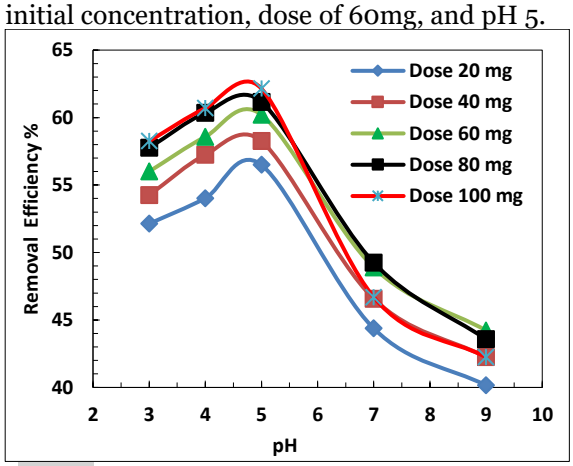

Fig. 9 Effect of pH on Removal Efficiency, C_i (10.7 mg/L), and CT =105.

3.3.Effect of Initial Concentration

Figure 10 shows that the PO_4^{-3} removal efficiency increased with the initial concentration because the driving force for adsorption increased with concentration. The removal efficiency stabilized with increasing the inlet concentration because most available adsorption sites were filled [30, 31]. Ibrahim and Jaddo [32] found that as the inlet pollutant concentration increased, the adsorbent was saturated much faster due to increasing the driving force. Li et al. [33] revealed that the required time to get equilibrium and the adsorbed mass were increased with the initial pollutant concentration due to increasing the driving force with the pollutant concentration. They also stated that there was a quick initial stage of adsorption followed by a slow stage due to the availability of a large number of adsorbent sites, and a greater driving force at the beginning of the process yielded higher mass transfer [34]. When equilibrium was approached, the pollutant concentration was

reduced, and the adsorption sites were mostly saturated, leading to a lower adsorption rate. This trend well agrees with that of [24-27], [35-38]. The best values for the removal efficiency were 68.22% for C_i of 10.7 mg/L and Al_2O_3/ABGAC dose of 100 mg.

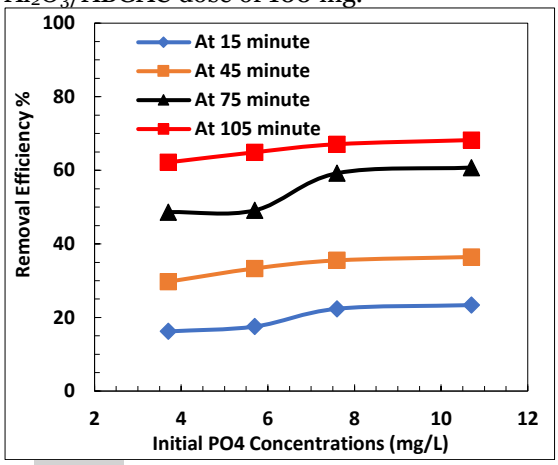

Fig. 10 Effect of Initial Concentrations on Removal Efficiency, Dose 100 mg, and pH 5.

3.4.Effect of Dose

Figure 11 represents the effect of the Al_2O_3/ABGAC dose on PO_4^{-3} removal. The PO_4^{-3} removal usually improved when the adsorbent doses were increased because a higher dose provides greater adsorption sites. The maximum PO_4^{-3} removal was 68.22 % at 100 mg dose, and C_i =10.7 mg/L. This result also indicated that the equilibrium conditions were reached after a certain dose. Elkhaleefa et al. [26] found that the removal efficiency increased with the adsorbent mass due to the increase in the surface area. Ragheb [39] stated that the removal efficiency increased with the increase in dose. The author attributed this increase to the increase in surface area. The maximum PO_4^{-3} removal was 68.22 % at 100 mg dose and C_i =10.7 mg/L. This behavior is consistent with [20, 33, 34], [40-42].

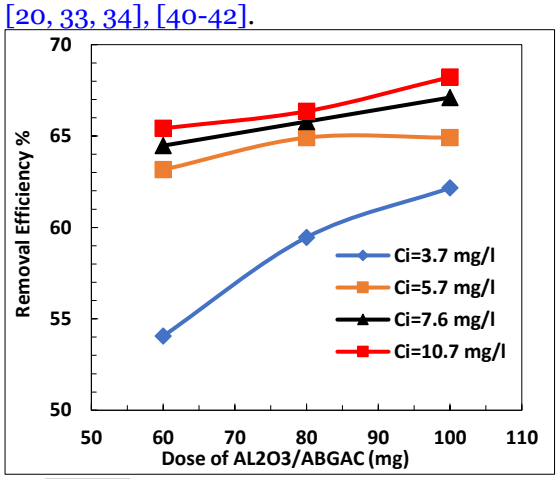

Fig. 11 Effect of Al2O3/ABGAC Dose on Removal Efficiency, 105 Minutes, and pH 5.

3.5.Effect of Magnetic Flux

Figure 12 shows that the PO_4^{-3} removal increased with the magnetic field strength. Increasing the magnetic flux up to 600 mTesla would make PO_4^{-3} more magnetic, increasing the attraction force. Even though phosphate is not magnetic, it is affected by a magnetic field. Where magnetic saturation happens, no further effect will be gained. Several studies explained that water properties are affected by magnetic treatment since this treatment affects the molecular and physicochemical properties of water [43]. Alimi et al. [44] concluded that the magnetic treatment would change the water's crystalline shape and put water in a state of supersaturation. This state allows the start of salt crystallization and agglomeration to form large crystals that are easy to deposit [45, 46]. Baker and Judd [47] showed that increasing magnetic flux intensity would increase pollutant removal due to the agglomeration of particles due to the change in electric dipole, which will affect the physical properties of water. Many works [48-50] proved that the pollutant removal efficiency increased with the magnetic flux. The highest phosphate removal efficiency was 73.68% at 600 mTesla at 60 mg dose, and C_i =7.6 mg/L. This trend agrees well with [51-54]. However, Ahmad and Dixit [55] found that the increasing magnetic field intensity from 0.7 to 7 T showed low improvement in phosphate removal.

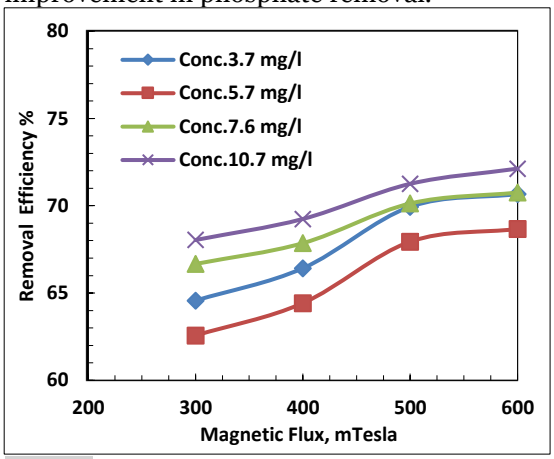

Fig. 12 Effect of MFS on Removal Efficiency at CT=105 Minute, pH =5, and Dose 100 mg.

3.6.Effect of Light

Pavel et al. [56] stated that removing harmful chemicals by photocatalysis has great interest. However, this method has many disadvantages, including low reaction rates. Thus, the present set was divided into two stages to investigate the effect of contact time on phosphate removal efficiency under red and blue light and six wavelengths on phosphate removal.

3.6.1.Determine the New Contact Time

Figure 13 shows the impact of time on the removal efficiency at red and blue lights. It is worth mentioning that the effect of light on adsorption processes did not appear during a short period. Therefore, longer periods were tested to determine the new contact time using a near and direct halogen light at two

wavelengths, blue (450-510) nm and red (650-720) nm using PO_4^{-3} initial concentration of 5.7 and 10.7 mg/L under the best working conditions found in earlier schemes, which are; pH 5, Al_2O_3/ABGAC dose of 80, 100 mg, and magnetic field intensity of 600 mTesla. Figure 13 indicated that approximately 70% of the phosphates were removed during the first hours. However, the rise was slow until it stabilized after 7 hours. Careful inspection of the results of many works (for example, [57-63]) indicated that photocatalysis consists of many reactions, some of which are slow and require a long time. Moreover, these reactions were relatively fast at the beginning. Then, it was slowed down with time since the reaction rate depends on the pollutant concentration and the intensity of light [60].

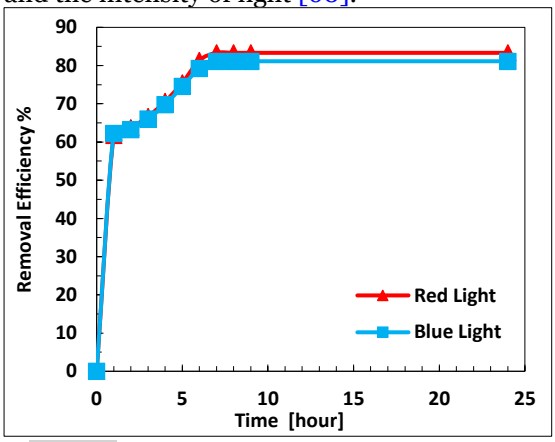

Fig. 13 Effect of Contact Time on Removal Efficiency at MFS 600 mTesla, pH= 5, Ci =10.7 mg/L, and Dose 100 mg.

3.6.2.Effect of Wavelength

Many experiments were conducted to test the effect of wavelength on PO_4 removal. The investigated wavelengths were red, 650-720 nm; yellow, 560-590 nm; Green, 510-560 nm; blue, 450-510; white, 390-710 nm; and sunlight, 400-750 nm. Figure 14 indicates that the removal efficiency increased with the contact time. It was found that 70% of the total removal occurred within the first hour. Then, the increase became slow and small until 7-8 hours, then stabilized. The results showed that up to 80% of PO_4 can be removed when exposed to different types of light due to the photocatalysis process that would enhance photocatalytic reactions between Al_2O_3/ABGAC and light. The photocatalytic activity of Al_2O_3/ABGAC under different lights depends mainly on the interface concentration. Those interfaces separated electron-hole pairs due to light irradiation [64].

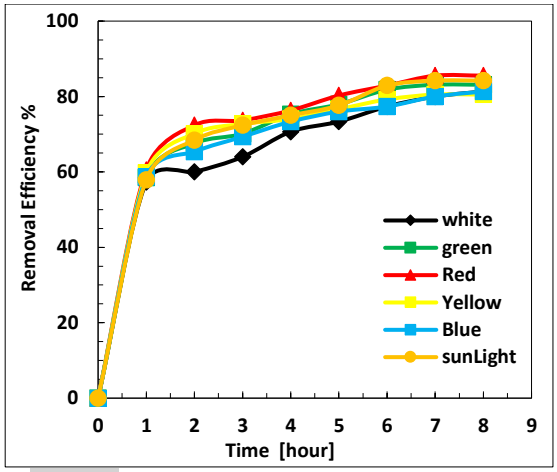

Fig. 14 Effect of Contact Time on Removal Efficiency, Ci=7.6 mg/L, Dose 60 mg, MFS 600 mTesla, and pH= 5.

The Al_2O_3/ABGAC has good photocatalytic efficiency due to its large bandgap. In addition, the Al^{3+} surface has specific sites for acidic O_2 photo adsorption. Thus, Al_2O_3/ABGAC can be induced to photoactivate O_2 [65]. This photoactivation is based on generating the electron-hole pairs (e^-- h^+) under the effect of light energy greater than the bandgap [66]. This trend agrees well with that of [25]. Illuminating a sample by different light sources having photon energy higher than that of the band gap of ABGAC will photoexcite electrons and holes in the conduction band (CB) and valence band (VB) of ABGAC, respectively, since the lowest energy level of the CB of ABGAC was higher than that of the new equilibrium Fermi energy level (E_f) of Al_2O_3/ABGAC, the electrons on the CB transferred from ABGAC to Al_2O_3. This transfer of electrons can be made possible only by doping Al_2O_3 with ABGAC. The charge separation resulted from the Schottky barrier. Schottky barriers have to rectify characteristics and are suitable for use as a diode. One of the primary characteristics of a Schottky barrier is the Schottky barrier, height which depends on the metal and semiconductor formed at the metal-semiconductor interface [67]. Thus, Al_2O_3NPs acted as electron sinks, reducing the recombination of photo-generated electrons and holes and prolonging the lifetime of the electron-hole pairs. The photo-generated electrons can reduce the phosphate molecules or react with electron acceptors, such as O_2 adsorbed on the AL(III) surface or dissolved in water, thereby reducing phosphate molecules to the superoxide radical anion $O^{\cdot -2}$ [68]. The red color had the highest removal of 85.52% at C_i=7.6 mg/L, Al_2O_3/ABGAC dose (60 mg), CT=8-hour, MFS =600 mTesla, and pH 5. Figure 15 shows that the removal efficiency for the six colors was slightly different. Different colors affected removal efficiency differently due to the pyramidal shape formed by loading the nanomaterial on the activated carbon.

These materials possess enhanced strength for photocatalytic activity due to their high surface area, high porosity, unique electronic properties, surface function groups, and narrow energy bandgap values, which lead to the color effect according to the wavelength of each color [69]. Therefore, the red color was more effective in increasing the removal rate due to the relatively narrow and high wavelength.

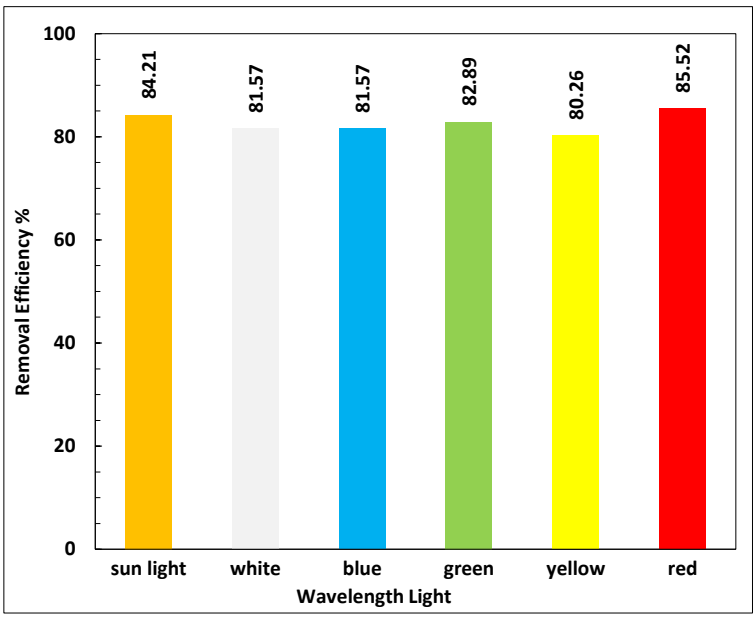

Fig. 15 Effect of Wavelength on Removal Efficiency, [Ci=7.6mg/L, Dose 60 mg, CT=8 Hours, MFS =600 mTesla, and pH =5.

3.8.Adsorption Isotherm Models

Many models were used to represent adsorption data. Freundlich and Langmuir models (Eqs. (3) and (4), respectively) are the most widely used models.

$$\text{Freundlich model Log } X/M = \text{Log } k + 1/n \log C \quad (3)$$

$$\text{Langmuir models } C/(X/M) = 1/ab + (1/b)\, C \quad (4)$$

The Correlation coefficient (R^2) ranges for the Freundlich and Langmuir models are (0.9083-0.9937) and (0.9219-0.9981), respectively, meaning that the Langmuir model well fitted the experimental data. Thus, this model was used to calculate the adsorption capacity. It was found that the calculated adsorption capacity range was (63.24 - 969.38) mg/g. For the results of both models, constants are tabulated in Table 3 and shown in Fig. 16 and Fig. 17.

Table 3 Constants of Freundlich and Langmuir Models.

Dose of Al_2O_3/ ABGAC mg	Equilibrium concentration mg/L	Freundlich constants			Langmuir constants		
		n	k	R^2	a	b	R^2
Initial concentration of PO4 = 3.7 mg/l, CT = 105 min, pH = 5, MFS =600 mT and Red light							
20	0.957	-0.57431	224.698	0.9083	-0.67608	17.4216	0.9313
40	0.955	-0.64913	106.267	0.9201	-0.73092	10.7642	0.9344
60	0.926	-0.68481	61.9298	0.9169	-0.75074	6.64011	0.9323
80	0.936	-0.84363	39.4729	0.9303	-0.82156	6.56167	0.9312
100	0.945	-0.59428	43.2613	0.911	-0.70847	3.65764	0.9219
Initial concentration of PO4 = 5.6 mg/l, CT = 105 min, pH = 5, MFS =600 mT and Red light							
20	0.957	-2.42071	241.3237	0.9937	-2.12121	142.8574	0.9981
40	0.955	-2.49438	119.6189	0.9853	-2.20634	71.94244	0.9963
60	0.926	-2.49003	79.67091	0.9895	-0.45454	47.84688	0.9963
80	0.936	-2.60078	59.23794	0.98	-0.45441	41.66666	0.9748
100	0.945	-2.71444	47.08688	0.9862	-0.40540	30.03003	0.9959

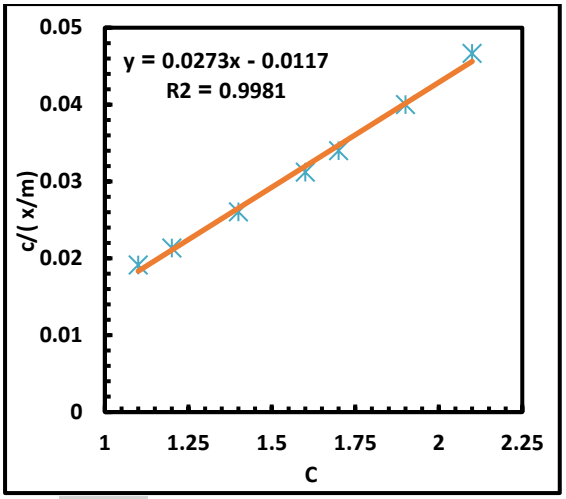

Fig. 16 Adsorption Data According to Langmuir Model, Ci=5.6mg/L, dose 80mg, and pH =5.

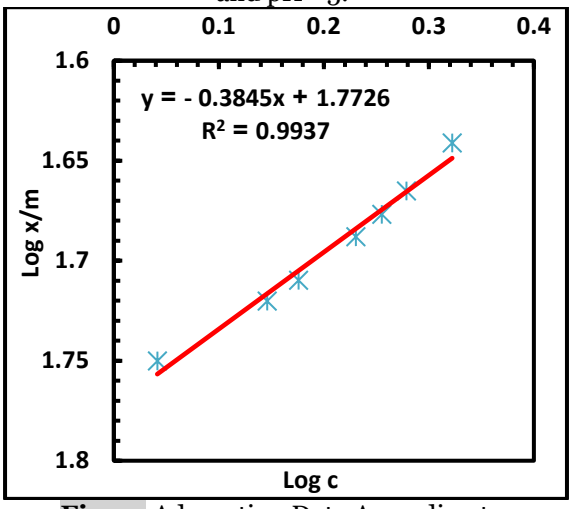

Fig. 17 Adsorption Data According to Freundlich Model, Ci=5.6mg/L, Dose 80mg, and pH =5.

3.8.1.Effect of Al_2O_3/ABGAC Dose on Adsorption Capacity

Figure 18 represents the effect of AL_2O_3/ABGAC dose on the adsorption capacity at pH of 5, at initial phosphate concentration C_i of 3.7-10.7 mg/l, contact time of 105 minutes, magnetic field strength 600 mTesla. Figure 18 indicates that increasing the adsorbent dose increased the adsorption capacity. The maximum adsorption capacity was 969.387 (mg/g) at the initial phosphate concentration of 7.6 mg/L. According to the Langmuir model, the term X/M reduced as the dose increased. So, the term C/(X/M) increases with the dose, increasing the adsorption capacity. These results agree with that [8, 70, 80].

3.8.2.Effect of Initial PO_4^{-3} Concentration on Adsorption Capacity

Figure 19 shows the effect of initial concentration on adsorption capacity at a pH of 5 for a dose of 20-100 mg/L under a contact time of 105 min. It is noticed that the adsorption capacity increased with the decrease in initial phosphate concentration. The maximum adsorption capacity was 960.344 (mg/g) at a dose of 60 mg. The driving force of adsorption is the difference between the initial and equilibrium concentrations. The driving force increased with the initial concentration, increasing the adsorbed mass(X). Thus, X/M for constant dose increased. Therefore, C/(X/M) decreased, i.e., adsorption capacity decreased. Several researchers, i.e., Tee et al. [71], Di et al. [72], Farouq [73], and Sen [74]), stated that the adsorbed amount increased with the initial concentration due to the increase in the driving force. Albadarin et al. [75] and Di et al. [72] found that higher initial concentrations resulted in a higher chance of collisions with adsorption sites. In addition, increasing the driving force reduced the mass transfer resistance. These results agree well with that of [76].

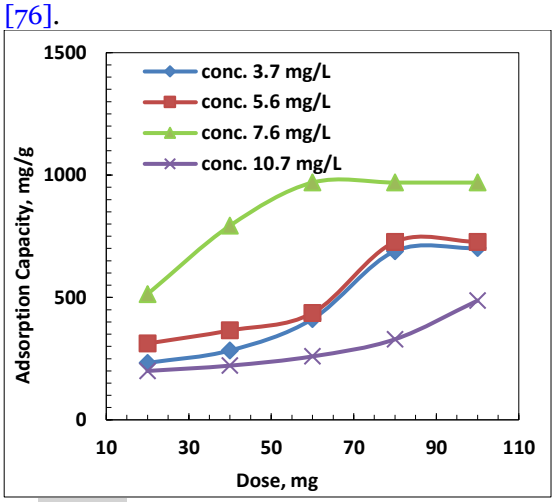

Fig. 18 Effect of AL2O3/ABGAC Dose on Adsorption Capacity at MFS 600mT, CT =105 Minute, and Red Light.

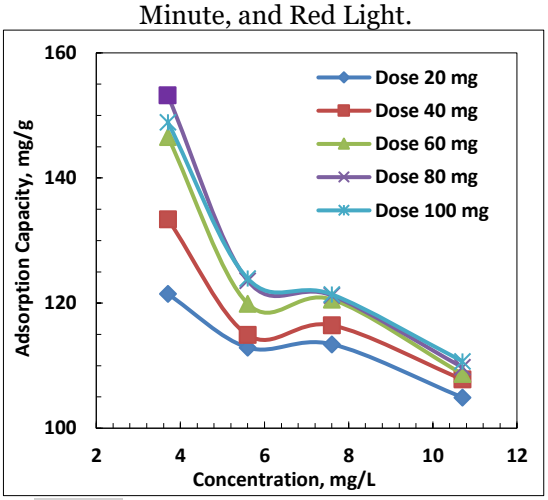

Fig. 19 Effect of Initial Concentration on Adsorption Capacity, MFS=600mT, CT=105 Minutes, pH=5, and Red Light.

3.8.3.Effect of pH on Adsorption Capacity

Figure 20 indicates that the adsorption capacity increased with pH until pH=5. Then, the adsorption capacity decreased for further increase in pH. The highest adsorption capacity occurred at pH =5 and a dose of 60 mg was

969.38 mg/g. This behavior happens due to two opposite forces. The first is the driving force that increases the adsorbed amount X. Increasing X increases the term (X/M) and thus reduces C/(X/M), i.e., reducing adsorption capacity. The second force results from the change of the surface and ionic structure of the adsorbent, making it more attractive to phosphate near pH =5 and rendering the adsorbent less attractive to phosphate far from pH =5. This behavior will act as if the adsorption sites increased near pH =5 and decreased when pH was away from 5 in both directions. This behavior acts as if M increases, reducing X/M that increases C/(X/M). It seems that the resultant of these two opposite forces increases adsorption capacity since the second force is greater than the first force. When pH was higher than 5, the first force exceeded the second. Cozmuta [77] found that when pH decreased from 4 to 1, the adsorption capacity reduced due to the competition between hydrogen ions and the ions under investigation at low pH of Argun [78]. Adeolu et al. [79] proved that the adsorption capacity increased with pH then decreased. They concluded that increasing pH decreased H+, reducing competition forces between pollutants and adsorption sites. Moreover, increasing pH encouraged the formation of soluble hydroxyl complexes that decreased the adsorption. Low et al. [80] found that adsorption depended on pH and concentration, with pH 4·5 being the optimum value. Das et al. [76] showed that a pH of 5 yielded the best adsorption result. These results agree well with that of [81].

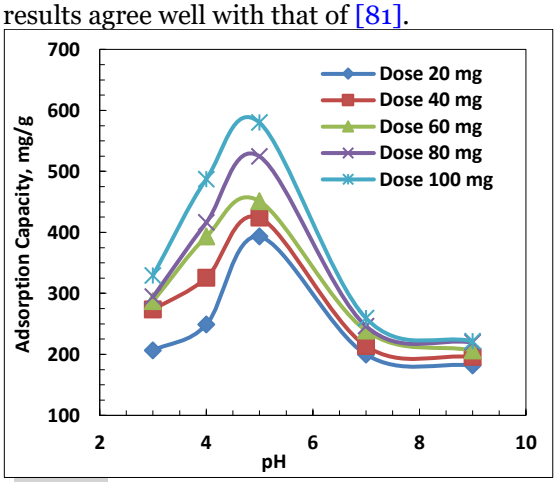

Fig. 20 Effect of pH on Adsorption Capacity, MFS 600mT, CT=105 Minutes, Ci =10.7 mg/L, and Red Light.

3.8.4.Effect of Wavelength Light on Adsorption Capacity

Al_2O_3/ABGAC, recognized for their photocatalytic activity, are materials that can be used differently. In this experiment, the photocatalytic activity of the Al_2O_3/ABGAC was tested to see how well it removed phosphate at the best experimental settings pH=5, dose 60–80 mg, and concentration of 3.7 and 7.6 mg/L (Fig. 21). This Figure shows that the maximum adsorption capacity was 969.3877(mg/g) at the dose of 60 mg, PO_4^{-3}, concentration 7.6 mg/L, magnetic field strength 600 mTesla, pH =5, and red light. Photoactivation plays an important role in increasing the adsorption sites' readiness to adsorb pollutants, acting as if M increases so that X/M will be reduced [69]. Consequently, C/(X/M) increased. Therefore, the adsorption capacity increased. In the present work, it seems that the red light resulted in the highest activation level, while green, white, and blue light resulted in the lowest activation. These results agree well with that of [82].

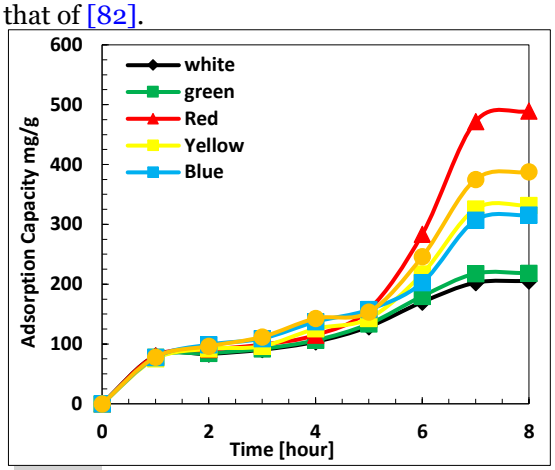

Fig. 21 Effect of Contact Time on Adsorption Capacity, MFS =600 mTesla, pH =5, Dose of 80 mg, and Ci= 7.6 mg/L.

3.9.The Kinetics of Adsorption

Examining adsorption kinetics plays a crucial role in determining the adsorption rate. Numerous models have been developed to address this, encompassing the pseudo-first-order, pseudo-second-order, intraparticle diffusion, mixed-order (M-O), and Elovich models. According to the pseudo-first-order model, the extent of adsorption is directly proportional to the quantity of active adsorption sites on the adsorbent material. On the other hand, the pseudo-second-order model delineates the rate-determining step of the adsorption process and specifies the nature of the bonds formed between the adsorbate and the adsorbent through chemisorption [83]. The equation that results in the pseudo-first-order kinetic model is as follows:

$$\mathbf{Log\ (q_e - q_t) = Log\ q_e - K_1 t} \qquad \mathbf{(5)}$$

It is possible to write the pseudo-second-order kinetic model as follows:

$$\frac{t}{q_t} = \frac{1}{K_2 q_e^2} + \frac{t}{q_e} \qquad \mathbf{(6)}$$

where K_1(min $^{-1}$) and K_2 (g.mg^{-1}.min $^{-1}$) are the rate constants of the pseudo-first-order and pseudo-second-order kinetic model equations, q_e is the total of adsorbed material at equilibrium (mg. g $^{-1}$), q_t is the total of adsorbed at time t (mg. g $^{-1}$) [84], and t is irradiation time (hour).

Table 4 Fitting Parameters of Phosphate Adsorption onto Zr(IV)-AS Using Pseudo-First-Order and Pseudo-Second-Order Kinetic Models [85].

C_o	q_e	pseudo-first order equation			pseudo-second-order equation		
($mg.L^{-1}$)	($mg.g^{-1}$)	K_1 (min^{-1})	q_e($mg.g^{-1}$)	R^2	K_2($mg.g^{-1}.min^{-1}$)	q_e($mg.g^{-1}$)	R^2
3.6	104.333	3.10×10^{-3}	103.331	0.9821	3.95×10^{-4}	114.64	0.9994
5.6	86.35	2.47×10^{-3}	69.566	0.9245	2.30×10^{-4}	79.68	0.9993
7.6	112.6	1.25×10^{-3}	97.568	0.9877	1.56×10^{-4}	103.25	0.9969
10.6	75	1.36×10^{-3}	47.586	0.9869	2.68×10^{-4}	61.235	0.9978

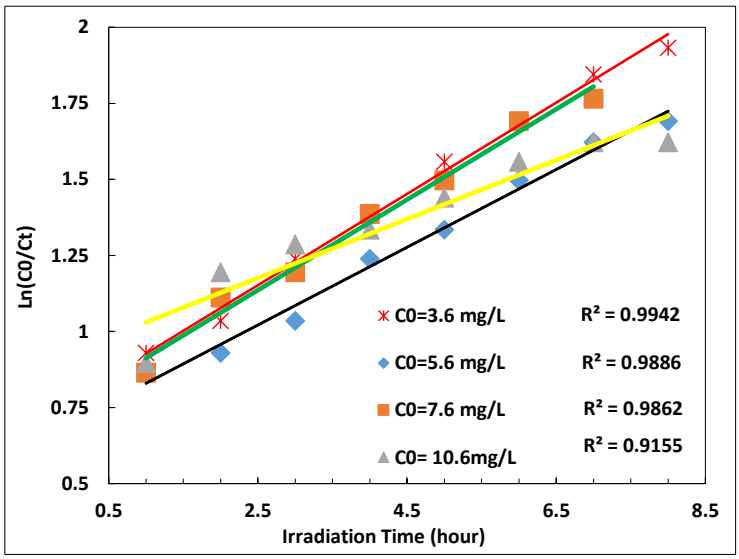

Fig. 22 The Pseudo-First-Order Plot, Red Light, AL2O3/ABGAC Active Dose, MFS 600 mTesla, CT= 8 Hours, and pH =5.

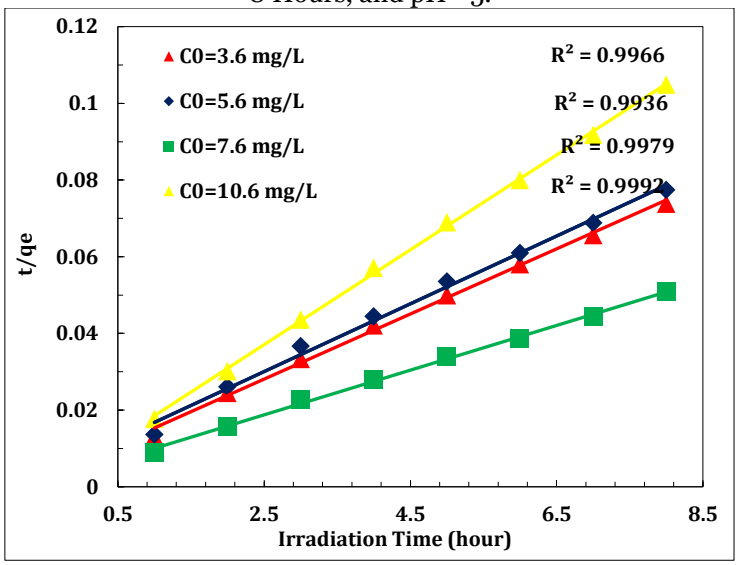

Fig. 23 The Pseudo-Second-Order Plot, Red Light, AL2O3/ABGAC Active Dose, MFS =600 mTesla, CT= 8 Hour, and pH=5.

From Table 4 and Figs. 22 and 23, it is clear that the correlation coefficient (R^2) for the pseudo-second-order model was higher than that of the pseudo-first-order kinetic model, meaning that the pseudo-second-order model fitted the experimental data.

4.CONCLUSIONS

This study showed that Al_2O_3/ABGAC was highly efficient in removing phosphate from synthetic aqueous solutions. It yielded a removal efficiency of 85.52%. It was also found that pH had the most significant effect, with the maximum removal efficiency at 7.6 mg/L initial concentration, dose of 60mg, and pH 5. However, the magnetic field and light slightly affected phosphate removal. The highest phosphate removal efficiency, i.e., C_i =7.6 mg/L, at 600 mTesla and red light at 60 mg dose. It was found that the adsorption capacity increased with the decrease of initial concentration and is directly proportional to the dose of Al_2O_3/ABGAC. Langmuir model significantly fitted with the adsorption data. The adsorption capacity range was 63.24 - 969.38 mg/g.

ACKNOWLEDGEMENTS

The authors highly appreciate the staff of the Chemical Engineering Department, College of

Engineering, Tikrit University. Appreciation is also devoted to the staff of the laboratories of the Environmental Engineering Department, College of Engineering, Tikrit University, according to the university order for admission to the study No. 3/7/9147 on 7/27/2021. Ministry of Water Resources is highly appreciated for their help in providing adequate information.

NOMENCLATURE

ABGAC	Aloe vera Barbadensis Gum Activated Carbon
a, b	Constants of Langmuir.
ATP	Adenosine triphosphate
C_o	Outlet concentration (mg/L)
CB	Conduction band
C_e	Equilibrium concentration (mg/L)
C_i	Initial concentration (mg/L)
CT	Contact time (hour, minute)
e^-	Electron energy
E_f	Fermi level
h^-	Hole pairs
K	Freundlich's constant
M	mass of the adsorbent (mg/L)
MOFs	Metal-organic frameworks
MONPs	Metal oxide nanoparticles
NPs	Nanoparticles
pH	Indicates how acidic or basic a substance is, and the scale ranges from 0 to 14
ppm	parts per million
R%	Removal efficiency
R^2	Correlation coefficient
RO	Reverse osmosis
t	Time (hour, minute)
TSP	Trisodium phosphate with the chemical formula Na_3PO_4
UiO-66	A metal organic framework made up of [Zr6O4(OH)4] clusters with 1,4-benzodicarboxylic acid struts
V	Solution volume (L)
VB	Valence band
X	Amount of adsorbent (mg/L)
XRD	X-ray diffractometers
Greek Letters	
γ, δ, θ, η, κ, α, β	Metastable phases of Al2O3 depending on the temperature

REFERENCES

[1] Schindler DW, Carpenter SR, Chapra SC, Hecky RE, Orihel DM. **Reducing Phosphorus to Curb Lake Eutrophication is a Success.** *Environmental Science & Technology* 2016; **50**(17):8923-8929.

[2] Chen M, Graedel TE. **A Half-Century of Global Phosphorus Flows, Stocks, Production, Consumption, Recycling, and Environmental Impacts.** *Global Environmental Change* 2016; **36**:139-152.

[3] Roy ED. **Phosphorus Recovery and Recycling with Ecological Engineering: A Review.** *Ecological Engineering* 2017; **98**:213-227.

[4] Tuszynska A, Kolecka K, Quant B. **The Influence of Phosphorus Fractions in Bottom Sediments on Phosphate Removal in Semi-Natural Systems as the 3rd Stage of Biological Wastewater Treatment.** *Ecological Engineering* 2013; **53**:321-328.

[5] Azam HM, Alam ST, Hasan M, Yameogo DS, Kannan AD, Rahman A, Kwon MJ. **Phosphorous in the Environment: Characteristics with Distribution and Effects, Removal Mechanisms, Treatment Technologies, and Factors Affecting Recovery as Minerals in Natural and Engineered Systems.** *Environmental Science and Pollution Research* 2019; **26**:20183-20207.

[6] Ray JR, Tadepalli S, Nergiz SZ, Liu KK, You L, Tang Y, Singamaneni S, Jun YS. **Hydrophilic, Bactericidal Nanoheater-Enabled Reverse Osmosis Membranes to Improve Fouling Resistance.** *ACS Applied Materials & Interfaces* 2015; **7**(21):11117-11126.

[7] Li G, Gao S, Zhang G, Zhang X. **Enhanced Adsorption of Phosphate from Aqueous Solution by Nanostructured Iron (III)–Copper (II) Binary Oxides.** *Chemical Engineering Journal* 2014; **235**:124-131.

[8] Lin KYA, Chen SY, Jochems AP. **Zirconium-Based Metal Organic Frameworks: Highly Selective Adsorbents for Removal of Phosphate from Water and Urine.** *Materials Chemistry and Physics* 2015; **160**:168-176.

[9] Wang Z, Xing M, Fang W, Wu D. **One-Step Synthesis of Magnetite Core/Zirconia Shell Nanocomposite for High Efficiency Removal of Phosphate from Water.** *Applied Surface Science* 2016; **366**:67-77.

[10] Zhang C, Li Y, Wang F, Yu Z, Wei J, Yang Z, Ma C, Li Z, Xu Z, Zeng G. **Performance of Magnetic Zirconium-Iron Oxide Nanoparticle in the Removal of Phosphate from Aqueous Solution.** *Applied Surface Science* 2017; **396**:1783-1792.

[11] Itrogiannis D, Psychoyou M, Baziotis I, Inglezakis VJ, Koukouzas N, Tsoukalas N, Palles D, Kamitsos E, Oikonomou G, Markou GM. **Removal of Phosphate from Aqueous Solutions by Adsorption onto Ca (OH) 2 Treated Natural Clinoptilolite.** *Chemical Engineering Journal* 2017; **320**:510-522.

[12] Xiong W, Tong J, Yang Z, Zeng G, Zhou Y, Wang D, Song P, Xu R, Zhang C, Cheng M. **Adsorption of Phosphate from Aqueous Solution Using Iron-Zirconium Modified Activated Carbon Nanofiber: Performance and Mechanism.** *Journal of Colloid and Interface Science* 2017; **493**:17-23.

[13] Manikandan V, Lee JH, Velmurugan P, Jayanthi P, Chang WS, Park YJ, Cho M, Oh BT. **Fabrication and Characterization of TiO 2-Loaded Moringa Oleifera Gum-Activated Carbon and the Photo-Catalytic Degradation of Phosphate in Aqueous Solutions.** *Nanotechnology for Environmental Engineering* 2018; **3**:1-13.

[14] Asfaram A, Ghaedi M, Agarwal S, Tyagi I, Gupta VK. **Removal of Basic Dye Auramine-O by ZnS: Cu Nanoparticles Loaded on Activated Carbon: Optimization of Parameters Using Response Surface Methodology with Central Composite Design.** *RSC Advances* 2015; **5**(24):18438-18450.

[15] Mukherjee S, Mukhopadhyay S, Zafri MZ, Zhan X, Hashim MA, Gupta B. **Application of Guar Gum for the Removal of Dissolved Lead from Wastewater.** *Industrial Crops and Products* 2018; **111**:261-269.

[16] Sahraei R, Pour ZS, Ghaemy M. **Novel Magnetic Bio-Sorbent Hydrogel Beads Based on Modified Gum Tragacanth/Graphene Oxide: Removal of Heavy Metals and Dyes from Water.** *Journal of Cleaner Production* 2017; **142**:2973-2984.

[17] Ragupathy S, Sathya T. **Synthesis and Characterization of SnO 2 Loaded on Groundnut Shell Activated Carbon and Photocatalytic Activity on MB Dye under Sunlight Radiation.** *Journal of Materials Science: Materials in Electronics* 2016; **27**:5770-5778.

[18] Velu M, Balasubramanian B, Velmurugan P, Kamyab H, Ravi AV, Chelliapan S, Lee CT, Palaniyappan J. **Fabrication of Nanocomposites Mediated from Aluminium Nanoparticles/Moringa Oleifera Gum Activated Carbon for Effective Photocatalytic Removal of Nitrate and Phosphate in Aqueous Solution.** *Journal of Cleaner Production* 2021; **281**:124553.

[19] Tamamushi BI. **Factors Influencing the Adsorption from Solutions.** *Adsorption from Solution* 1983; 79-86.

[20] Cundari L, Saputra E, Suranto A, Yandriani Y, Rosalina R. **The Effect of Adsorbent Type and Ratio on Removal and Isotherm Adsorption of Methylene Blue.** *Indonesian Journal of Materials Science* 2020; **21**(3):488354.

[21] Khader EH, Mohammed TJ, Mirghaffari N, Salman AD, Juzsakova T, Abdullah TA. **Removal of Organic Pollutants from Produced Water by Batch Adsorption Treatment.** *Clean Technologies and Environmental Policy* 2022; **24**(2):713-720.

[22] Al-Doury M, Ali SS. **Removal of Phenol and Parachlorophenol from Synthetic Wastewater Using Prepared Activated Carbon from Agricultural Wastes.** *International Journal of Sustainable and Green Energy* 2015; **4**(3):92-101.

[23] Jewell DM, Weber JH, Bunger JW, Plancher H, Latham DR. **Ion-Exchange, Coordination, and Adsorption Chromatographic Separation of Heavy-End Petroleum Distillates.** *Analytical Chemistry* 1972; **44**(8):1391-1395.

[24] Weber WJ. **Physicochemical Processes for Water Quality Control.** *Wiley Interscience* 1972; **9**:261-304.

[25] Kumar PS, Prabavathi SL, Indurani P, Karuthapandian S, Muthuraj V. **Light Assisted Synthesis of Hierarchically Structured Cu/CdS Nanorods with Superior Photocatalytic Activity, Stability and Photocatalytic Mechanism.** *Separation and Purification Technology* 2017; **172**:192-201.

[26] Elkhaleefa A, Ali IH, Brima EI, Shigidi I, Elhag AB, Karama B. **Evaluation of the Adsorption Efficiency on the Removal of Lead (II) Ions from Aqueous Solutions Using Azadirachta Indica Leaves as an Adsorbent.** *Processes* 2021; **9**(3):559.

[27] Ibrahim S, Ang HM, Wang S. **Removal of Emulsified Food and Mineral Oils from Wastewater Using Surfactant Modified Barley Straw.** *Bioresource Technology* 2009; **100**(23):5744-5749.

[28] Ali IH, Al Mesfer MK, Khan MI, Danish M, Alghamdi MM. **Exploring Adsorption Process of Lead (II) and Chromium (VI) Ions from Aqueous Solutions on Acid Activated Carbon Prepared from Juniperus Procera Leaves.** *Processes* 2019; **7**(4):217.

[29] Alasadi A, Khaili F, Awwad A. **Adsorption of Cu (II), Ni (II) and Zn (II) Ions by Nano Kaolinite: Thermodynamics and Kinetics Studies.** *Chemistry International* 2019; **5**(4):226-258.

[30] Ali I, Peng C, Ye T, Naz I. **Sorption of Cationic Malachite Green Dye on Phytogenic Magnetic Nanoparticles Functionalized by 3-Marcaptopropanic Acid.** *RSC Advances* 2018; **8**(16):8878-8897.

[31] Shaterabadi Z, Nabiyouni G, Soleymani M. **Correlation Between Effects of the**

Particle Size and Magnetic Field Strength on the Magnetic Hyperthermia Efficiency of Dextran-Coated Magnetite Nanoparticles. *Materials Science and Engineering* 2020; **117**:111274.

[32] Ibrahim MM, Jaddo IA. **Removal of Some Hydrocarbon Pollutants from Baiji Oil Refinery Wastewater Using Granular Activated Carbon Column.** *Tikrit Journal of Engineering Sciences* 2014; **21**(3):84-95.

[33] Li C, Yu Y, Li Q, Zhong H, Wang S. **Kinetics and Equilibrium Studies of Phosphate Removal from Aqueous Solution by Calcium Silicate Hydrate Synthesized from Electrolytic Manganese Residue.** *Adsorption Science & Technology* 2019; **37**(7-8):547-565.

[34] Zhang G, Liu H, Liu R, Qu J. **Removal of Phosphate from Water by a Fe–Mn Binary Oxide Adsorbent.** *Journal of Colloid and Interface Science* 2009; **335**(2):168-174.

[35] Lin SH, Wang CS. **Treatment of High-Strength Phenolic Wastewater by a New Two-Step Method.** *Journal of Hazardous Materials* 2002; **90**(2):205-216.

[36] Waleed MA. **Designing of Pilot for Treatment of Waste Water Contaminated by Furfural.** M.Sc Thesis, University of Baghdad, Baghdad, Iraq, 2004.

[37] Babu BV, Ramakrishna V. **Dominant Design Variables and Modeling Parameters for Adsorption in Batch Studies.** *International Symposium & 57th Annual Session of IIChE in Association with AIChE (CHEMCON-2004)*, Mumbai, 2004.

[38] Waadalla K. **Removal of Multi-Pollutant from Waste Water by Adsorption Method.** Ph.D. Thesis, University of Baghdad, Baghdad, Iraq, 2006.

[39] Ragheb SM. **Phosphate Removal from Aqueous Solution Using Slag and Fly Ash.** *HBRC Journal* 2013; **9**(3):270-275.

[40] Koumanova B, Drame M, Popangelova M. **Phosphate Removal from Aqueous Solutions Using Red Mud Wasted in Bauxite Bayer's Process.** *Resources, Conservation and Recycling* 1997; **19**(1):11-20.

[41] Cheraghipour E, Pakshir M. **Environmentally Friendly Magnetic Chitosan Nano-Biocomposite for Cu (II) Ions Adsorption and Magnetic Nano-Fluid Hyperthermia: CCD-RSM Design.** *Journal of Environmental Chemical Engineering* 2021; **9**(2): 104883.

[42] Sulaymon AH, Mohammed AA, Al-Musawi TJ. **Competitive Biosorption of Lead, Cadmium, Copper, and Arsenic Ions Using Algae.** *Environmental Science and Pollution Research* 2013; **20**:3011-3023.

[43] Fathi A, Mohamed T, Claude G, Maurin G, Mohamed BA. **Effect of a Magnetic Water Treatment on Homogeneous and Heterogeneous Precipitation of Calcium Carbonate.** *Water Research* 2006; **40**(10):1941-1950.

[44] Alimi F, Tlili M, Amor MB, Gabrielli C, Maurin G. **Influence of Magnetic Field on Calcium Carbonate Precipitation.** *Desalination* 2007; **206**(1-3):163-168.

[45] Cai R, Yang H, He J, Zhu W. **The Effects of Magnetic Fields on Water Molecular Hydrogen Bonds.** *Journal of Molecular Structure* 2009; **938**(1-3):15-19.

[46] Aldoury MMI, Ismaeal NN, Mahdi MJ. **Softening of Groundwater at Samarra City by Electromagnetic Polarization.** *IOP Conference Series: Earth and Environmental Science* 2022; **1120**:12009.

[47] Baker JS, Judd SJ. **Magnetic Amelioration of Scale Formation.** *Water Research* 1996; **30**(2):247-260.

[48] AL-Ibady QAK. **Influence of the Dipolar Magnetized Water on the Ecological Factors of Freshwater Ostracod Cypris Laevis (OF Müller, 1776).** *Journal of Environmental Science, Toxicology and Food Technology* 2015; **9**(9):9-15.

[49] Abdulrazzaq GH. **Reducing the Water Hardness by Using Electromagnetic Polarization Method.** *Al-Khwarizmi Engineering Journal* 2016; **12**(4):111-116.

[50] Al Helal A, Soames A, Gubner R, Iglauer S, Barifcani A. **Influence of Magnetic Fields on Calcium Carbonate Scaling in Aqueous Solutions at 150 C and 1 Bar.** *Journal of Colloid and Interface Science* 2018; **509**:472-484.

[51] Jain M, Yadav M, Kohout T, Lahtinen M, Garg VK, Sillanpää M. **Development of Iron Oxide/Activated Carbon Nanoparticle Composite for the Removal of Cr (VI), Cu (II) and Cd (II) Ions from Aqueous Solution.** *Water Resources and Industry* 2018; **20**:54-74.

[52] Zhu D, Hong X, Hui KS. **Magnetically Attracted Iron Scrap Anode Based Electrocoagulation for Phosphate Removal.** *Water Science and Technology* 2021; **84**(1):216-224.

[53] Yahya FH. **Using of Magnetic Nanoparticles to Remove Cu +2 from Aqueous Solution.** M.Sc Thesis, Tikrit University, Tikrit, Iraq, 2006.

[54] AbdelHady RS, Younes MA, Ibrahim AM, AbdelAziz MM. **An Empirical Model for Salt Removal Percentage in Water Under the Effect of Different Current Intensities of Current Carrying Coil at Different Flow Rates.** *Journal of Advanced Research* 2011; **2**(4):351-355.

[55] Shaikh AMH, Dixit SG. **Removal of Phosphate from Waters by Precipitation and High Gradient Magnetic Separation.** *Water Research* 1992; **26**(6):845-852.

[56] Pavel M, Anastasescu C, State RN, Vasile A, Papa F, Balint I. **Photocatalytic Degradation of Organic and Inorganic Pollutants to Harmless End Products: Assessment of Practical Application Potential for Water and Air Cleaning.** *Catalysts* 2023; **13**(2):380.

[57] Kosanić MM. **Photocatalytic Degradation of Oxalic Acid Over TiO2 Power.** *Journal of Photochemistry and Photobiology A: Chemistry* 1998; **119**(2):119-122.

[58] Muggli DS, McCue JT, Falconer JL. **Mechanism of the Photocatalytic Oxidation of Ethanol on TiO2.** *Journal of Catalysis* 1998; **173**(2):470-483.

[59] Yu Z, Chuang SS. **In Situ IR Study of Adsorbed Species and Photogenerated Electrons During Photocatalytic Oxidation of Ethanol on TiO2.** *Journal of Catalysis* 2007; **246**(1):118-126.

[60] Karunakaran C, Dhanalakshmi R. **Photocatalytic Performance of Particulate Semiconductors under Natural Sunshine—Oxidation of Carboxylic Acids.** *Solar Energy Materials and Solar Cells* 2008; **92**(5):588-593.

[61] de Bem Luiz D, Andersen SLF, Berger C, José HJ, Moreira RFP. **Photocatalytic Reduction of Nitrate Ions in Water Over Metal-Modified TiO2.** *Journal of Photochemistry and Photobiology A: Chemistry* 2012; **246**:36-44.

[62] Zhang Z, Wang W, Wang L, Sun S. **Enhancement of Visible-Light Photocatalysis by Coupling with Narrow-Band-Gap Semiconductor: A Case Study on Bi2S3/Bi2WO6.** *ACS Applied Materials & Interfaces* 2012; **4**(2):593-597.

[63] Raciulete M, Papa F, Kawamoto D, Munteanu C, Culita DC, Negrila C, Atkinson I, Bratan V, Pandele-Cusu J, Balint I. **Particularities of Trichloroethylene Photocatalytic Degradation over Crystalline RbLaTa2O7 Nanowire Bundles Grown by Solid-State Synthesis Route.** *Journal of Environmental Chemical Engineering* 2019; **7**(1):102789.

[64] Deng XZ, Song C, Tong YL, Yuan G, Gao F, Liu DQ, Zhang ST. **Enhanced Photocatalytic Efficiency of C 3 N 4/BiFeO 3 Heterojunctions: The Synergistic Effects of Band Alignment and Ferroelectricity.** *Physical Chemistry Chemical Physics* 2018; **20**(5):3648-3657.

[65] Yao K, Li J, Shan S, Jia Q. **One-Step Synthesis of Urchinlike SnS/SnS2 Heterostructures with Superior Visible-Light Photocatalytic Performance.** *Catalysis Communications* 2017; **101**:51-56.

[66] Pathania D, Katwal R, Sharma G, Naushad M, Khan MR, Ala'a H. **Novel Guar Gum/Al2O3 Nanocomposite as an Effective Photocatalyst for the Degradation of Malachite Green Dye.** *International Journal of Biological Macromolecules* 2016; **87**:366-374.

[67] Liu Y, Guo J, Zhu E, Liao L, Lee S, Ding M, Shakir I, Gambin V, Huang Y, Duan X. **Approaching the Schottky–Mott Limit in van der Waals Metal–Semiconductor Junctions.** *Nature* 2018; **557**(7707):696-700.

[68] Srivastava RR, Kim M, Lee J, Ilyas S. **Liquid–Liquid Extraction of Rhenium (VII) from an Acidic Chloride Solution Using Cyanex 923.** *Hydrometallurgy* 2015; **157**:33-38.

[69] Diacon A, Mocanu A, Răducanu CE, Busuioc C, Şomoghi R, Trică B, Dinescu A, Rusen E. **New Carbon/ZnO/Li2O Nanocomposites with Enhanced Photocatalytic Activity.** *Scientific Reports* 2019; **9**(1):16840.

[70] Salmani MH, Abedi M, Mozaffari SA, Sadeghian HA. **Modification of Pomegranate Waste with Iron Ions a Green Composite for Removal of Pb from Aqueous Solution: Equilibrium, Thermodynamic and Kinetic Studies.** *AMB Express* 2017; **7**(1):1-8.

[71] Tee GT, Gok XY, Yong WF. **Adsorption of Pollutants in Wastewater via Biosorbents, Nanoparticles and Magnetic Biosorbents: A Review.** *Environmental Research* 2022; **212**:113248.

[72] Di J, Ruan Z, Zhang S, Dong Y, Fu S, Li H, Jiang G. **Adsorption Behaviors and Mechanisms of Cu2+, Zn2+ and**

Pb2+ by Magnetically Modified Lignite. *Scientific Reports* 2022; **12**(1):1394.

[73] Farouq R. **Coupling Adsorption-Photocatalytic Degradation of Methylene Blue and Maxilon Red.** *Journal of Fluorescence* 2022; **32**(4):1381-1388.

[74] Sen TK. **Adsorptive Removal of Dye (Methylene Blue) Organic Pollutant from Water by Pine Tree Leaf Biomass Adsorbent.** *Processes* 2023; **11**(7):1877.

[75] Albadarin AB, Mangwandi C, Ala'a H, Walker GM, Allen SJ, Ahmad MNM. **Kinetic and Thermodynamics of Chromium Ions Adsorption onto Low-Cost Dolomite Adsorbent.** *Chemical Engineering Journal* 2012; **179**:193-202.

[76] Das J, Patra BS, Baliarsingh N, Parida KM. **Adsorption of Phosphate by Layered Double Hydroxides in Aqueous Solutions.** *Applied Clay Science* 2006; **32**(3-4):252-260.

[77] Cozmuta LM, Cozmuta AM, Peter A, Nicula C, Nsimba EB, Tutu H. **The Influence of pH on the Adsorption of Lead by Na-Clinoptilolite: Kinetic and Equilibrium Studies.** *Water SA* 2012; **38**(2):269-278.

[78] Argun ME. **Use of Clinoptilolite for the Removal of Nickel Ions from Water: Kinetics and Thermodynamics.** *Journal of Hazardous Materials* 2008; **150**(3):587-595.

[79] Adeolu AT, Okareh OT, Dada AO. **Adsorption of Chromium Ion from Industrial Effluent Using Activated Carbon Derived from Plantain (Musa Paradisiaca) Wastes.** *American Journal of Environmental Protection* 2016; **4**(1):7-20.

[80] Low KS, Lee CK, Leo AC. **Removal of Metals from Electroplating Wastes Using Banana Pith.** *Bioresource Technology* 1995; **51**(2-3):227-231.

[81] Subratti A, Vidal JL, Lalgee LJ, Kerton FM, Jalsa NK. **Preparation and Characterization of Biochar Derived from the Fruit Seed of Cedrela Odorata L and Evaluation of its Adsorption Capacity with Methylene Blue.** *Sustainable Chemistry and Pharmacy* 2021; **21**:100421.

[82] Romero Saez M, Jaramillo LY, Saravanan R, Benito N, Pabón E, Mosquera E, Caroca FG. **Notable Photocatalytic Activity of TiO2 - Polyethylene Nanocomposites for Visible Light Degradation of Organic Pollutants.** *eXPRESS Polymer Letters* 2017; **11**(11):899-909.

[83] Simonin JP. **On the Comparison of Pseudo-First Order and Pseudo-Second Order Rate Laws in the Modeling of Adsorption Kinetics.** *Chemical Engineering Journal* 2016; **300**:254-263.

[84] Guo X, Wang J. **A General Kinetic Model for Adsorption: Theoretical Analysis and Modeling.** *Journal of Molecular Liquids* 2019; **288**:111100.

[85] Wang J, Tong X, Wang S. **Zirconium-Modified Activated Sludge as a Low-Cost Adsorbent for Phosphate Removal in Aqueous Solution.** *Water, Air, & Soil Pollution* 2018; **229**:1-10.